

## Real-Time *GW*: Toward an *Ab Initio* Description of the Ultrafast Carrier and Exciton Dynamics in Two-Dimensional Materials

E. Perfetto<sup>1,2</sup>, Y. Pavlyukh<sup>1</sup>, and G. Stefanucci<sup>1,2</sup>

<sup>1</sup>*Dipartimento di Fisica, Università di Roma Tor Vergata, Via della Ricerca Scientifica 1, 00133 Rome, Italy*

<sup>2</sup>*INFN, Sezione di Roma Tor Vergata, Via della Ricerca Scientifica 1, 00133 Rome, Italy*



(Received 30 September 2021; accepted 18 November 2021; published 4 January 2022)

We demonstrate the feasibility of the time-linear scaling formulation of the *GW* method [Phys. Rev. Lett. **124**, 076601 (2020)] for *ab initio* simulations of optically driven two-dimensional materials. The time-dependent *GW* equations are derived and solved numerically in the basis of Bloch states. We address carrier multiplication and relaxation in photoexcited graphene and find deviations from the typical exponential behavior predicted by the Markovian Boltzmann approach. For a resonantly pumped semiconductor we discover a self-sustained screening cascade leading to the Mott transition of coherent excitons. Our results draw attention to the importance of non-Markovian and dynamical screening effects in out-of-equilibrium phenomena.

DOI: [10.1103/PhysRevLett.128.016801](https://doi.org/10.1103/PhysRevLett.128.016801)

In the last two decades the *GW* approximation [1] has emerged as a successful and popular tool for describing at microscopic level electronic and optical properties of quantum matter. The merits of this method arise from the proper inclusion of dynamical and nonlocal effects, leading to band structures and absorption spectra in excellent agreement with experiments in a broad class of materials [2,3].

The nonequilibrium extension of the *GW* approximation would be of utmost importance to address several ultrafast phenomena; its implementation, however, has been so far computationally too prohibitive. The real-time *GW* method is based on the numerical solution of the Kadanoff-Baym equations (KBE) for the one-particle Green's function (GF). As the method scales cubically with the physical propagation time [4–6], the *GW* KBE have only been solved in model systems [7–11] and confined to very short timescales [12,13]. The timescaling does not improve with the generalized Kadanoff-Baym ansatz (GKBA) [14], and simulations up to few hundreds of femtoseconds have been restricted to jelliumlike models [15–17].

A significant advance has been recently achieved with a time-linear scaling formulation of the *GW*-GKBA approach [18,19]. The *GW*-GKBA equations have been mapped onto a coupled system of ordinary differential equations (ODE) for the one-particle density matrix and the equal-time two-particle GF. The ODE scheme (also applicable to second-Born, *T* matrix [18,19] and other correlated methods [20,21]) preserves the full non-Markovian nature of the dynamics, and successful tests in small finite systems are already available [18,19,21].

In this Letter we extend and solve numerically the *GW*-ODE scheme for spatially periodic two-dimensional (2D) systems, thus opening the way to *ab initio* real-time *GW*

simulations in material science. We investigate two different materials to highlight different aspects of the *GW* method. First we reexamine the problem of carrier multiplication in photoexcited graphene [22–28]. By comparison with Boltzmann equation (BE) results, we show that the (so far neglected) non-Markovian effects modify considerably the impact ionization dynamics. The second application concerns with the photogenerated screening in 2D semiconductors. Pumping resonantly with the exciton energy [29–31], we find that there is a critical excitation density above which the coherent exciton superfluid melts abruptly (coherent exciton Mott transition) well before phonon-induced decoherence takes places [32]. This is due to a self-sustained screening cascade, a phenomenon that can be captured only if the screened electron-hole (*e-h*) attraction is properly updated during the evolution.

*Real-time GW formalism.*—We consider a periodic system with  $N_b$  bands and denote by  $V_{lnmi}^{\mathbf{q}\mathbf{k}\mathbf{k}'}$  the scattering amplitude for two electrons in bands  $m$  and  $i$  with quasimomenta  $\mathbf{k}' + \mathbf{q}$  and  $\mathbf{k} - \mathbf{q}$  to end up in the bands  $n$  and  $l$  with quasimomenta  $\mathbf{k}'$  and  $\mathbf{k}$  respectively, see Fig. 1(a). Let us introduce the spin-symmetric lesser and greater GFs  $G_{\mathbf{k}ij}^<(t,t') = i\langle c_{\mathbf{k}j\sigma}^\dagger(t')c_{\mathbf{k}i\sigma}(t) \rangle$  and  $G_{\mathbf{k}ij}^>(t,t') = -i\langle c_{\mathbf{k}i\sigma}(t)c_{\mathbf{k}j\sigma}^\dagger(t') \rangle$ , where  $\hat{c}_{\mathbf{k}i\sigma}^{(\dagger)}$  annihilates (creates) an electron with quasimomentum  $\mathbf{k}$  and spin  $\sigma$  in band  $i$ . The inclusion of spin-orbit and the generalization to spin-dependent GFs is straightforward. The goal of this work is to study the temporal evolution of the one-particle density matrix  $\rho_{\mathbf{k}ij}(t) \equiv -iG_{\mathbf{k}ij}^<(t,t)$  in the *GW* approximation. By defining  $\Sigma_{\mathbf{k}}(t,t')$  as the *GW* self-energy, see Fig. 1(b), the equation of motion to solve is

$$\frac{d\rho_{\mathbf{k}}(t)}{dt} = -i[h_{\mathbf{k}}(t), \rho_{\mathbf{k}}(t)] - I_{\mathbf{k}}(t) - I_{\mathbf{k}}^{\dagger}(t), \quad (1)$$

$$I_{\mathbf{k}}(t) = \int dt' [\Sigma_{\mathbf{k}}^{\geq}(t, t') G_{\mathbf{k}}^{\leq}(t', t) - \Sigma_{\mathbf{k}}^{\leq}(t, t') G_{\mathbf{k}}^{\geq}(t', t)], \quad (2)$$

where all quantities are  $N_b \times N_b$  matrices in the band indices. The time-dependent single-particle Hamiltonian reads [33]

$$h_{\mathbf{k}ij}(t) = \delta_{ij}\epsilon_{\mathbf{k}i} + P_{\mathbf{k}ij}(t) + \sum_{\mathbf{k}'mn} (2V_{imnj}^{0\mathbf{k}\mathbf{k}'} - V_{imjn}^{(\mathbf{k}-\mathbf{k}')\mathbf{k}\mathbf{k}'}) \delta\rho_{\mathbf{k}'nm}(t), \quad (3)$$

where the  $\epsilon_{\mathbf{k}i}$  are the band dispersions of a preliminary equilibrium  $GW$  calculation whereas  $P_{\mathbf{k}ij}(t)$  describes the coupling of the electrons to an external field. The last term in Eq. (3) is the variation of the Hartree-Fock potential due to the variation ( $\delta\rho$ ) of the density matrix with respect to the equilibrium value  $\rho_{\mathbf{k}nm}^{\text{eq}} = \delta_{nm}f(\epsilon_{\mathbf{k}n})$ , with  $f$  the zero-temperature Fermi-Dirac distribution.

We implement the GKBA [14] to obtain a closed equation for  $\rho$ , i.e., we express the lesser and greater GFs as  $G_{\mathbf{k}}^{\lessgtr}(t, t') = -G_{\mathbf{k}}^R(t, t')\rho_{\mathbf{k}}^{\lessgtr}(t') + \rho_{\mathbf{k}}^{\lessgtr}(t)G_{\mathbf{k}}^A(t, t')$ , where we have defined  $\rho_{\mathbf{k}}^{\leq} = \rho_{\mathbf{k}}$  and  $\rho_{\mathbf{k}}^{\geq} = \rho_{\mathbf{k}} - \mathbb{1}$ . The retarded and advanced propagators are approximated at the quasi-particle level, hence  $G_{\mathbf{k}}^R(t, t') = -i\theta(t-t')T\{e^{-i\int_{t'}^t dt h_{\mathbf{k}}(t)}\}$  ( $T$  being the time-ordering operator) and  $G_{\mathbf{k}}^A(t, t') = [G_{\mathbf{k}}^R(t', t)]^{\dagger}$ . The bottleneck in solving Eq. (1) is the numerical evaluation of the  $GW$  self-energy  $\Sigma_{\mathbf{k}ij}^{\lessgtr}(t, t') = i\sum_{\mathbf{q}mn} W_{imjn}^{\lessgtr\mathbf{q}\mathbf{k}(\mathbf{k}-\mathbf{q})}(t, t')G_{\mathbf{k}-\mathbf{q}nm}^{\lessgtr}(t, t')$  since the screened interaction  $W(t, t')$  obeys the random phase approximation integral equation for every  $t$  and  $t'$ , making the overall numerical scaling cubic in the propagation time.

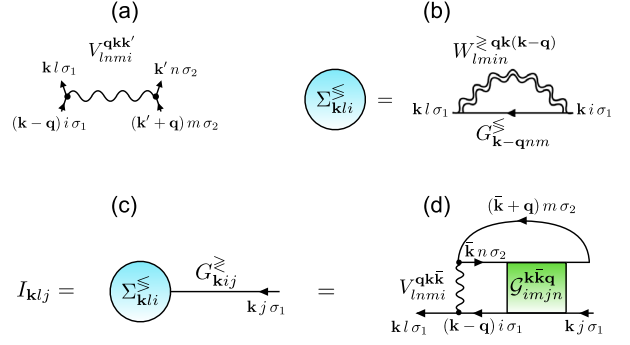


FIG. 1. Diagrammatic representation of the Coulomb scattering amplitude (a),  $GW$  self-energy (b) and collision integral in terms of the self-energy (c), and two-particle GF (d).

Remarkably, however, such scaling can be reduced from cubic to linear through the simultaneous propagation of the two-particle GF  $\mathcal{G}$  [18,19].

The collision integral  $I(t)$  in Eq. (2), see also Fig. 1(c), can equivalently be written in terms of  $\mathcal{G}$  as illustrated in Fig. 1(d):

$$I_{\mathbf{k}lj}(t) = -i\sum_{\substack{\mathbf{k}\mathbf{q} \\ imn}} \mathcal{G}_{imjn}^{\mathbf{k}\mathbf{k}\mathbf{q}}(t) \mathcal{V}_{ni}^{(-\mathbf{q})\bar{\mathbf{k}}\mathbf{k}}, \quad (4)$$

where  $\mathcal{G}_{lm}^{\mathbf{k}\mathbf{k}'\mathbf{q}} \equiv \mathcal{G}_{lm}^{\mathbf{k}\mathbf{k}'\mathbf{q}}$  and  $\mathcal{V}_{lm}^{\mathbf{q}\mathbf{k}\mathbf{k}'} \equiv V_{lmni}^{\mathbf{q}\mathbf{k}\mathbf{k}'}$  are matrices (two-index tensors) in the space of pairs of band indices [34]. Henceforth we use boldface letters to denote matrices in this space. Introducing also the matrices  $\mathbf{h}_{\mathbf{k}\mathbf{k}',lm}(t) \equiv h_{\mathbf{k}lm}(t)\delta_{in} - h_{\mathbf{k}'ni}(t)\delta_{lm}$  and  $\rho_{\mathbf{k}\mathbf{k}',lm}^{\lessgtr}(t) \equiv \rho_{\mathbf{k}lm}^{\lessgtr}(t)\rho_{\mathbf{k}'ni}^{\lessgtr}(t)$  we obtain a compact equation of motion for the two-particle GF [34]:

$$i\frac{d}{dt}\mathcal{G}^{\mathbf{k}\bar{\mathbf{k}}\mathbf{q}}(t) = -2[\rho_{(\mathbf{k}-\mathbf{q})\mathbf{k}}^{\geq}(t)\mathcal{V}^{\mathbf{q}(\mathbf{k}-\mathbf{q})(\bar{\mathbf{k}}+\mathbf{q})}\rho_{\bar{\mathbf{k}}(\bar{\mathbf{k}}+\mathbf{q})}^{\leq}(t) - \rho_{(\mathbf{k}-\mathbf{q})\mathbf{k}}^{\leq}(t)\mathcal{V}^{\mathbf{q}(\mathbf{k}-\mathbf{q})(\bar{\mathbf{k}}+\mathbf{q})}\rho_{\bar{\mathbf{k}}(\bar{\mathbf{k}}+\mathbf{q})}^{\geq}(t)] + \mathbf{h}_{(\mathbf{k}-\mathbf{q})\mathbf{k}}(t)\mathcal{G}^{\mathbf{k}\bar{\mathbf{k}}\mathbf{q}}(t) - \mathcal{G}^{\mathbf{k}\bar{\mathbf{k}}\mathbf{q}}(t)\mathbf{h}_{\bar{\mathbf{k}}(\bar{\mathbf{k}}+\mathbf{q})}(t) + 2\sum_{\mathbf{k}'} [\mathcal{G}^{\mathbf{k}\mathbf{k}'\mathbf{q}}(t)\mathcal{V}^{(-\mathbf{q})\mathbf{k}'(\bar{\mathbf{k}}+\mathbf{q})}\rho_{\bar{\mathbf{k}}(\bar{\mathbf{k}}+\mathbf{q})}^{\Delta}(t) - \rho_{(\bar{\mathbf{k}}-\mathbf{q})\mathbf{k}}^{\Delta}(t)\mathcal{V}^{(-\mathbf{q})(\mathbf{k}-\mathbf{q})\mathbf{k}'}\mathcal{G}^{\mathbf{k}'\bar{\mathbf{k}}\mathbf{q}}(t)] \equiv \mathcal{I}^{\mathbf{k}\bar{\mathbf{k}}\mathbf{q}}(t). \quad (5)$$

In Eq. (5)  $\rho_{\mathbf{k}\mathbf{k}'}^{\Delta} \equiv \rho_{\mathbf{k}\mathbf{k}'}^{\geq} - \rho_{\mathbf{k}\mathbf{k}'}^{\leq}$  and matrix multiplication between  $N_b^2 \times N_b^2$  matrices is understood. The second-Born (2B) approximation without the second-order exchange contribution is recovered by neglecting the last line of Eq. (5). If we instead set  $N_b = 1$  and choose  $V_{1111}^{\mathbf{q}\mathbf{k}\mathbf{k}'} = V^{\mathbf{q}}$  depending only on the transferred momentum  $\mathbf{q}$ , we recover the  $GW$  ODE for jellium [18,19].

Equations (1), (4), (5) form a closed system of first-order ODE that is equivalent to the original  $GW$ -GKBA scheme. Notice that in the  $GW$ -ODE scheme the  $GW$  self-energy

$\Sigma(t, t')$  is never evaluated. The collision integral  $\mathcal{I}(t)$  depends only on the instantaneous  $\mathcal{G}(t)$ ,  $\rho(t)$ , and  $\mathbf{h}(t)$ . The numerical scaling is linear in time, quartic in the number of  $\mathbf{k}$  points  $N_{\mathbf{k}}$  and sextic in the number of bands  $N_b$ . The scaling with  $N_{\mathbf{k}}$  can be reduced from quartic to cubic by working in localized bases, e.g., Wannier orbitals. In these bases the Coulomb tensor is well approximated by a sum of factorized contributions,  $V_{lmni}^{\mathbf{q}\mathbf{k}\mathbf{k}'} \approx \sum_{\alpha\beta} v^{\alpha\beta}(\mathbf{q})F_{li}^{\alpha}(\mathbf{k}, \mathbf{q})F_{nm}^{\beta}(\mathbf{k}', \mathbf{q})$ , where  $\alpha$  and  $\beta$  run over the number of (typically few) localized orbitals in the unit

cell. With such factorization the contraction over  $\mathbf{k}'$  in Eq. (5) can be executed only once for all  $\bar{\mathbf{k}}$ , thus lowering the  $N_{\mathbf{k}}$  scaling by one power and making *ab initio* real-time GW simulations affordable, as it has been demonstrated for BE-based methods in Refs. [35,36].

We have implemented the GW-ODE scheme in 2D systems having a single valence ( $i = 1$ ) and a single conduction ( $i = 2$ ) band (hence  $N_b = 2$ ). Accordingly, the equilibrium one-particle density matrix  $\rho_{\mathbf{k}11}^{\text{eq}} = 1$ ,  $\rho_{\mathbf{k}22}^{\text{eq}} = 0$ , and  $\rho_{\mathbf{k}12}^{\text{eq}} = 0$ . We use  $\rho_{\mathbf{k}}(0) = \rho_{\mathbf{k}}^{\text{eq}}$  as initial condition. To avoid double countings we also subtract from the right-hand side of Eq. (5) the contribution of initial correlations, already taken into account in the dressing of the GW band structures  $\epsilon_{\mathbf{k}i}$ . Hence we modify the equation of motion for  $\mathcal{G}$  according to  $i(d/dt)\mathcal{G}^{\mathbf{k}\bar{\mathbf{k}}\mathbf{q}}(t) = \mathcal{I}^{\mathbf{k}\bar{\mathbf{k}}\mathbf{q}}(t) - \mathcal{I}^{\mathbf{k}\bar{\mathbf{k}}\mathbf{q}}(0)$  and set  $\mathcal{G}^{\mathbf{k}\bar{\mathbf{k}}\mathbf{q}}(0) = 0$ . Although the equilibrium state is weakly correlated, the electron-electron interaction plays a crucial role in the photoexcited dynamics, see below. We solve numerically the GW-ODE equations for the GW and 2B approximations using the CHEERS code [37]. We also provide comparisons with results from the BE, i.e., the semiconductor Bloch equation [38] in the 2B-Markov approximation [34]. For the numerical simulations we use polar coordinates (centered in the minimum of the optically activated valleys)  $\mathbf{k} = (k, \theta)$ , where the modulus  $k$  (angle  $\theta$ ) varies on a uniform grid of  $N_k$  ( $N_\theta$ ) points between 0 and  $k_{\text{max}}$  ( $2\pi$ ). The linear-time propagation is performed using the fourth-order Runge-Kutta solver.

*Carrier multiplication in photoexcited graphene.*—Due to its semimetallic nature pristine graphene has scarce screening efficiency [39,40]. Moreover in Ref. [41] it has been shown that second-order exchange effects are negligible. We therefore expect that 2B and GW calculations give similar results and that the comparison between GW and BE well highlights the role of non-Markovian effects.

Previous studies have shown that immediately after the photoexcitation, the electron dynamics is dominated by the impact ionization [22,25,42–45]. This interband process promotes electrons from the valence to the conduction band at the expense of energy loss by photoexcited hot carriers. Due to the linearity of the Dirac spectrum, carrier multiplication can occur mainly via collinear scattering [44]. These scatterings, however, have a vanishingly small phase space (and therefore become irrelevant) if the energy of the quasiparticles is exactly conserved [44]. In the BE approach an empirical energy-broadening  $\eta$  [34] is therefore introduced to capture the effect.

For photoexcitations with photon energy  $\lesssim 3$  eV graphene is well described by the Dirac cone approximation [46], where conduction and valence bands have linear dispersion  $\epsilon_{\mathbf{k}1,2} = \pm v_F k$ , with  $v_F$  the Fermi velocity and  $k = |\mathbf{k}|$  a small momentum around the  $K(K')$  point of the first Brillouin zone. In this case the Coulomb integral has a simple expression [46]

$V_{lnmi}^{\mathbf{q}\mathbf{k}\mathbf{k}'} = (2\pi/\epsilon q)F_{il}(\theta_{\mathbf{k}-\mathbf{q}} - \theta_{\mathbf{k}})F_{mn}(\theta_{\mathbf{k}'+\mathbf{q}} - \theta_{\mathbf{k}'})$ , where  $F_{mn}(\theta) = \{[1 + (-1)^{m+n}e^{i\theta}]/2\}$ , with  $\theta_{\mathbf{k}}$  the polar angle of the momentum  $\mathbf{k}$ . We take a dielectric constant  $\epsilon \approx 2.5$ , originating from a typical insulating substrate like  $\text{SiO}_2$  [47].

We consider graphene initially in the ground state and then driven out of equilibrium by a pump field linearly polarized along a direction  $\mathbf{e}$  on the plane. The explicit form of the light-matter interaction term is [48]  $P_{kij}(t) = \delta_{i1}\delta_{j2}ME(t)[(k_x e_y - k_y e_x)/k]$ , where  $E(t) = \theta(1 - |1 - 2t/T_p|)E\sin^2(\pi t/T_p)\sin(\omega_p t)$  is the pump envelope with duration  $T_p = 20$  fs and frequency  $\omega_p = 1.5$  eV; the Rabi frequency  $M$  is varied in order to promote excitation densities in the range  $10^{10}$ – $10^{12}$  carriers/cm<sup>2</sup>. To improve convergence we have regularized the bare interaction  $1/q \rightarrow 1/(q + q_c)$ ; in the simulations  $q_c = 0.01 \text{ \AA}^{-1}$  is a small cutoff that can be understood as the Thomas-Fermi momentum ascribed to a small unintentional doping [49]. For a given valley ( $K$  or  $K'$ ) we have used  $N_k = 16$ ,  $N_\theta = 24$ , and  $k_{\text{max}} = 0.2 \text{ \AA}^{-1}$ . The real-time simulations have been performed with a time step  $\Delta t = 0.2$  fs up to 150 fs; at times  $\gtrsim 200$  fs intervalley scattering and electron-phonon interactions (which are neglected in our calculations) become relevant [43,44] and our results become less accurate. In Fig. 2(a) we show the evolution of the carrier density in the conduction band  $n(t) = (4/A) \sum_{\mathbf{k}} \rho_{\mathbf{k}22}(t)$  during and after the illumination, for different pump intensities. The factor 4 accounts for the spin and valley degeneracy while  $A = 5.1 \times 10^{-16} \text{ cm}^2$  is the unit-cell area of graphene. In order to illustrate the carrier multiplication effect as a function of the pump intensity we plot  $n(t)/n_P$ , where  $n_P \equiv n(T_p)$  is the excited density at the end of the pump. The GW simulation confirms the predicted behavior of a decrease in the rate

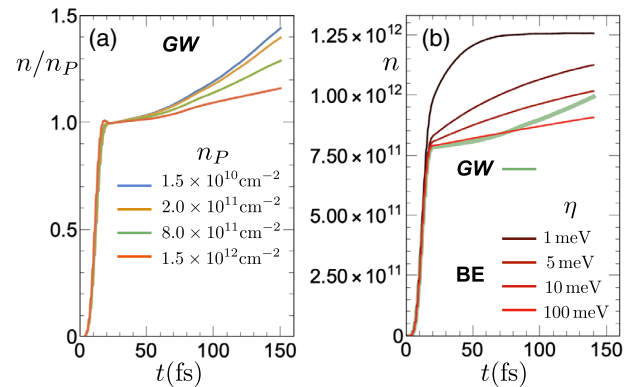


FIG. 2. (a) Time-dependent normalized carrier density  $n(t)/n_P$  in photoexcited graphene in the GW approximation for different pump intensities. (b) Carrier density  $n(t)$  (in units of  $\text{cm}^{-2}$ ) in the GW and BE approach for different values of the broadening  $\eta$ ; in all simulations we use the same pump intensity, giving  $n_P = 8 \times 10^{11} \text{ cm}^{-2}$  in the GW case.

of carrier multiplication with increasing the carrier density [22]. This is due to the Pauli blocking effect that reduces the phase space for impact ionization. Notice that no parameters (like  $\eta$  in the BE approach) appear in the *GW*-ODE scheme.

In Fig. 2(b) we compare the *GW* result to the BE outcome for different values of the broadening  $\eta$ . In all simulations we use the same pump intensity, giving  $n_p = 8 \times 10^{11} \text{ cm}^{-2}$  in the *GW* case. In the BE approach the carrier multiplication depends strongly on the chosen broadening. During illumination, energy is not conserved and therefore the smaller  $\eta$  is the less accurate description of the early transient dynamics. This explains why the BE curve obtained with the large value  $\eta = 0.1 \text{ eV}$  is the closest to *GW*. At larger times  $t \gtrsim 60 \text{ fs}$ , however, the two curves depart from each other. In particular the *GW* evolution does not follow (at least within this temporal window) the typical exponential saturation behavior of the BE, characterized by a downward concavity for  $t > T_p$ . This qualitative difference is due to non-Markovian effects as in this case the 2B results (see the Supplemental Material [34]) are very close to the *GW* ones.

In Fig. 3 we compare the evolution of the momentum-resolved occupations  $f_{\mathbf{k}}(t) = \rho_{\mathbf{k}22}(t)$  in different approaches. We clearly see that the carrier population is initially highly anisotropic due to the linear polarization of the pulse [43]. As already observed *GW* agrees well with BE for  $\eta = 0.1 \text{ eV}$  up to time  $t \approx 60 \text{ fs}$ , i.e., when the distribution is still anisotropic. At this time a substantial portion of the initial hot electrons have already migrated towards the Dirac point due to interparticle scattering. At larger times *GW* predicts a rapid thermalization while in BE the same process is much slower. The BE results are strongly affected by the value of  $\eta$ . At smaller  $\eta = 5 \text{ meV}$  the thermalization is very fast: there is a sizable charge

redistribution already during illumination, and at  $t \approx 60 \text{ fs}$  the distribution is essentially isotropic.

*Coherent excitons in semiconductors.*—A crucial feature of the real-time *GW* method is the updating of the screened interaction during the time evolution. We highlight this effect in a prototype 2D semiconductor hosting bound excitons inside the gap, and study the dynamics activated by pumping in resonance with the lowest excitonic energy. Resonant pumping creates a fluid of coherent excitons [50], characterized by long-lived monochromatic oscillations of the macroscopic polarization [51–57]. We here address the relaxation dynamics of the macroscopic polarization due to excited state screening. Let us model a direct-gap 2D semiconductor with band dispersions  $\epsilon_{\mathbf{k}1,2} = \pm \epsilon_g/2 \pm k^2/2m$ , where  $\epsilon_g$  is the band gap and  $m$  the effective mass of electrons and holes. In semiconductors the Coulomb integrals that do not conserve the particle number in each band are typically small [58] and can be neglected. In addition we assume a dependence only on the transferred momentum, i.e.,  $V_{lnmi}^{\mathbf{q}\mathbf{k}_1\mathbf{k}_2} = V^{\mathbf{q}}\delta_{li}\delta_{nm}$ , and take the standard 2D interaction  $V^{\mathbf{q}} = 2\pi/\epsilon(q+q_c)$ , where  $\epsilon$  accounts for the dielectric screening of the surrounding environment. Typical values to describe optical excitation in a monolayer transition metal dichalcogenide around the *K* valley are  $\epsilon_g = 2 \text{ eV}$ ,  $m = 0.5m_e$  ( $m_e$  being the electron mass) and  $\epsilon = 10$  (e.g., sapphire substrate). By solving the Bethe-Salpeter equation at equilibrium with these parameters we find the lowest energy exciton at  $\epsilon_x \approx 1.9 \text{ eV}$  (i.e., binding energy of  $0.1 \text{ eV}$ ). Real-time simulations have been performed using  $N_k = 32, N_\theta = 32$ . We adopted a momentum cutoff  $k_{\text{max}} = 0.3 \text{ \AA}^{-1}$  for excitation densities  $n_p \lesssim 5 \times 10^{11} \text{ cm}^{-2}$  while  $k_{\text{max}} = 0.5 \text{ \AA}^{-1}$  for  $n_p \gtrsim 5 \times 10^{11} \text{ cm}^{-2}$ , time step  $\Delta t = 0.025 \text{ fs}$ .

The system is excited with a laser pulse having the same envelope  $E(t)$  used for graphene but with a resonant frequency  $\omega_p = \epsilon_x = 1.9 \text{ eV}$  and duration  $T_p = 25 \text{ fs}$ . For simplicity we assume an isotropic excitation with momentum-independent light-matter interaction  $P_{\mathbf{k}ij}(t) = \delta_{i1}\delta_{j2}ME(t)$ . Accordingly the density matrix and all observables depend only on the modulus  $k$ . Also in this case the Rabi frequency is varied in order to promote excitation densities in the range  $10^{10}$ – $10^{12}$  carriers/ $\text{cm}^2$ . In Fig. 4(a) we show the evolution of the momentum-resolved carrier distribution  $f_{\mathbf{k}}(t) = \rho_{\mathbf{k}22}(t)$  for a low excited density  $n_p = (4/A) \sum_{\mathbf{k}} \rho_{\mathbf{k}22}(T_p) = 10^{11} \text{ cm}^{-2}$ —the characteristic value  $A = 9 \times 10^{-16} \text{ cm}^2$  has been used. During pumping excitons are predominantly created and  $f_{\mathbf{k}} \propto |Y_{\mathbf{k}}|^2$ , where  $Y_{\mathbf{k}}$  is the exciton wave function [30,31,57,59,60]. We have recently shown that for small excited densities the coherent exciton superfluid is not able to screen the Coulomb interaction [61]. As a consequence the  $e$ - $h$  attraction is not reduced and excitons survive for long time. The superfluid phase is characterized by a macroscopic polarization  $p(t) = \sum_{\mathbf{k}} \rho_{\mathbf{k}12}(t)$  that oscillates monochromatically at

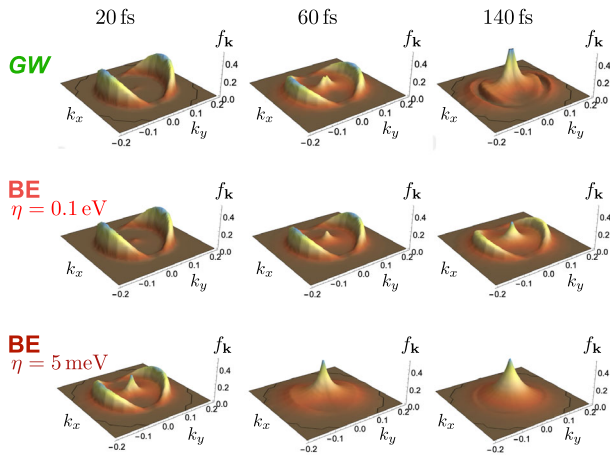


FIG. 3. Snapshots of the carrier distribution function  $f_{\mathbf{k}}$  in photoexcited graphene in *GW* (first row), BE for  $\eta = 100 \text{ meV}$  (second row) and BE  $\eta = 5 \text{ meV}$  (third row). Here the pump field is polarized along the  $x$  axis. Momenta  $k_x$  and  $k_y$  are in  $\text{\AA}^{-1}$ .

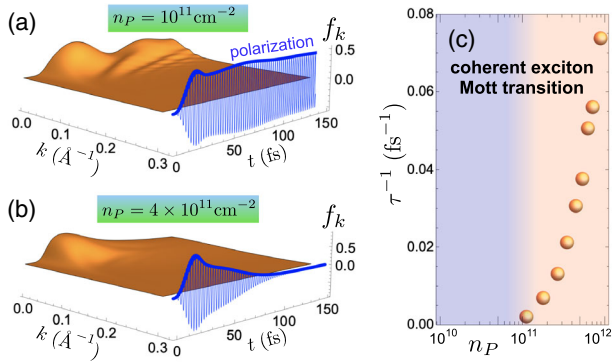


FIG. 4. Real-time GW evolution of the carrier distribution function  $f_k(t)$  in a 2D semiconductor for excitation density  $n_p = 10^{11} \text{ cm}^{-2}$  (a) and  $n_p = 4 \times 10^{11} \text{ cm}^{-2}$  (b). The time-dependent polarization  $p(t)$  (multiplied by a factor 2000) is also shown as a blue curve. In panel (c) we display the polarization inverse lifetime  $\tau^{-1}$  as a function of  $n_p$  (in units of  $\text{cm}^{-2}$ ). Here we used  $q_c = 0.02 \text{ \AA}^{-1}$ .

the exciton frequency  $\epsilon_x$  [57], see the blue curve in Fig. 4(a). In this regime no relaxation occurs, and the carrier occupations  $f_k(t)$  slowly attain the values reached at the end of the pump. The system thermalizes only at later times via electron-phonon scattering [62] (not considered in the present work).

The scenario changes dramatically at higher excited densities. In Fig. 4(b) we see that for  $n_p = 4 \times 10^{11} \text{ cm}^{-2}$  the polarization damps in about 100 fs, and after few femtoseconds ( $t \gtrsim 150 \text{ fs}$ ) the occupations  $f_k$  reach steady-state values describing a Fermi-Dirac distribution at temperature  $\sim 2000 \text{ K}$  (not shown), consistently with recent data [63]. We have systematically studied the lifetime of the polarization  $p(t)$  by varying the excitation density. In Fig. 4(c) we plot the inverse of the time  $\tau$  needed to reduce the amplitude of  $p(t)$  by one order of magnitude, as function of the carrier density  $n_p$ . No damping of the polarization can be detected for  $n_p \lesssim 10^{11} \text{ cm}^{-2}$ , while  $\tau^{-1}$  grows very fast beyond this threshold. The mechanism behind the described behavior is a screening cascade: (1) at sufficiently high excitation density the screening of the excitonic superfluid is nonvanishing and the effective  $e$ - $h$  attraction is reduced, (2) excitons start dissociating in a plasma of quasifree electrons in conduction band and quasifree holes in valence band, and (3) the  $e$ - $h$  plasma has a high screening efficiency and the  $e$ - $h$  attraction gets drastically reduced [60]. This self-sustained mechanism leads to a rapid melting of the superfluid state, signaled by a decay of the polarization. The thermalization occurs via scattering between incoherent quasiparticles, and the occupations  $f_k(t)$  relax towards a hot Fermi-Dirac distribution. We emphasize that this coherent exciton Mott transition is different from the well-known excitonic Mott transition [64–67], which refers to the breakdown of a system of incoherent excitons [68].

In conclusion we have demonstrated the feasibility of real-time GW simulations in 2D materials via the generalization and practical implementation of the recently proposed GW-ODE scheme [18,19]. The GW approximation gives easy access to so far neglected effects that we have shown to be crucial for the photoexcited many-electrons dynamics in graphene and 2D semiconductors. Although the method presented in this work applies exclusively to electronic processes, electron-phonon scatterings can be included without affecting the linear-time scaling [20]. This opens new avenues for the *ab initio* description and understanding of ultrafast phenomena observed in time-resolved experiments.

We acknowledge funding from MIUR PRIN Grant No. 20173B72NB and from INFN17-Nemesys project. G. S. acknowledges Tor Vergata University for financial support through the Mission Sustainability Project No. 2DUTOPI.

- [1] L. Hedin, New method for calculating the one-particle green's function with application to the electron-gas problem, *Phys. Rev.* **139**, A796 (1965).
- [2] L. Reining, The GW approximation: Content, successes and limitations, *Wiley Interdiscip. Rev.* **8**, e1344 (2018).
- [3] D. Golze, M. Dvorak, and P. Rinke, The GW compendium: A practical guide to theoretical photoemission spectroscopy, *Frontiers of chemistry : Proceedings of the Frontiers of Chemistry Conference* **7**, 377 (2019).
- [4] L. P. Kadanoff and G. A. Baym, *Quantum Statistical Mechanics: Green's Function Methods in Equilibrium and Nonequilibrium Problems* (Benjamin, New York, 1962).
- [5] G. Stefanucci and R. van Leeuwen, *Nonequilibrium Many-Body Theory of Quantum Systems: A Modern Introduction* (Cambridge University Press, Cambridge, England, 2013).
- [6] K. Balzer and M. Bonitz, *Nonequilibrium Green's Functions Approach to Inhomogeneous Systems* (Springer, New York, 2012).
- [7] P. Myöhänen, A. Stan, G. Stefanucci, and R. van Leeuwen, Kadanoff-Baym approach to quantum transport through interacting nanoscale systems: From the transient to the steady-state regime, *Phys. Rev. B* **80**, 115107 (2009).
- [8] P. Myöhänen, A. Stan, G. Stefanucci, and R. van Leeuwen, A many-body approach to quantum transport dynamics: Initial correlations and memory effects, *Europhys. Lett.* **84**, 67001 (2008).
- [9] M. Puig von Friesen, C. Verdozzi, and C.-O. Almbladh, Kadanoff-Baym dynamics of Hubbard clusters: Performance of many-body schemes, correlation-induced damping and multiple steady and quasi-steady states, *Phys. Rev. B* **82**, 155108 (2010).
- [10] M.P. von Friesen, C. Verdozzi, and C.-O. Almbladh, Successes and Failures of Kadanoff-Baym Dynamics in Hubbard Nanoclusters, *Phys. Rev. Lett.* **103**, 176404 (2009).
- [11] M. Schüler, J. Berakdar, and Y. Pavlyukh, Time-dependent many-body treatment of electron-boson dynamics:

- Application to plasmon-accompanied photoemission, *Phys. Rev. B* **93**, 054303 (2016).
- [12] D. Golež, M. Eckstein, and P. Werner, Multiband non-equilibrium  $GW$  + EDMFT formalism for correlated insulators, *Phys. Rev. B* **100**, 235117 (2019).
- [13] N. Bittner, D. Golež, M. Casula, and P. Werner, Photo-induced Dirac-cone flattening in  $\text{BaNiS}_2$ , *Phys. Rev. B* **104**, 115138 (2021).
- [14] P. Lipavský, V. Špička, and B. Velický, Generalized Kadanoff-Baym ansatz for deriving quantum transport equations, *Phys. Rev. B* **34**, 6933 (1986).
- [15] L. Bányai, Q. T. Vu, B. Mieck, and H. Haug, Ultrafast Quantum Kinetics of Time-Dependent RPA-Screened Coulomb Scattering, *Phys. Rev. Lett.* **81**, 882 (1998).
- [16] Q. T. Vu, H. Haug, W. A. Hügel, S. Chatterjee, and M. Wegener, Signature of Electron-Plasmon Quantum Kinetics in Gaas, *Phys. Rev. Lett.* **85**, 3508 (2000).
- [17] Q. T. Vu and H. Haug, Time-dependent screening of the carrier-phonon and carrier-carrier interactions in nonequilibrium systems, *Phys. Rev. B* **62**, 7179 (2000).
- [18] N. Schlünzen, J.-P. Joost, and M. Bonitz, Achieving the Scaling Limit for Nonequilibrium Green Functions Simulations, *Phys. Rev. Lett.* **124**, 076601 (2020).
- [19] J.-P. Joost, N. Schlünzen, and M. Bonitz, G1-G2 scheme: Dramatic acceleration of nonequilibrium Green functions simulations within the Hartree-Fock generalized Kadanoff-Baym ansatz, *Phys. Rev. B* **101**, 245101 (2020).
- [20] D. Karlsson, R. van Leeuwen, Y. Pavlyukh, E. Perfetto, and G. Stefanucci, Fast Green's Function Method for Ultrafast Electron-Boson Dynamics, *Phys. Rev. Lett.* **127**, 036402 (2021).
- [21] Y. Pavlyukh, E. Perfetto, and G. Stefanucci, Photoinduced dynamics of organic molecules using nonequilibrium Green's functions with second-Born,  $GW$ ,  $T$ -matrix, and three-particle correlations, *Phys. Rev. B* **104**, 035124 (2021).
- [22] T. Winzer, A. Knorr, and E. Malic, Carrier multiplication in graphene, *Nano Lett.* **10**, 4839 (2010).
- [23] J. C. W. Song, K. J. Tielrooij, F. H. L. Koppens, and L. S. Levitov, Photoexcited carrier dynamics and impact-excitation cascade in graphene, *Phys. Rev. B* **87**, 155429 (2013).
- [24] D. Brida, A. Tomadin, C. Manzoni, Y. J. Kim, A. Lombardo, S. Milana, R. R. Nair, K. S. Novoselov, A. C. Ferrari, G. Cerullo *et al.*, Ultrafast collinear scattering and carrier multiplication in graphene, *Nat. Commun.* **4**, 1987 (2013).
- [25] T. Plötzing, T. Winzer, E. Malic, D. Neumaier, A. Knorr, and H. Kurz, Experimental verification of carrier multiplication in graphene, *Nano Lett.* **14**, 5371 (2014).
- [26] K. Tielrooij, J. Song, S. A. Jensen, A. Centeno, A. Pesquera, A. Z. Elorza, M. Bonn, L. Levitov, and F. Koppens, Photoexcitation cascade and multiple hot-carrier generation in graphene, *Nat. Phys.* **9**, 248 (2013).
- [27] S. Tani, F. Blanchard, and K. Tanaka, Ultrafast Carrier Dynamics in Graphene Under a High Electric Field, *Phys. Rev. Lett.* **109**, 166603 (2012).
- [28] J. C. Johannsen, S. Ulstrup, A. Crepaldi, F. Cilento, M. Zacchigna, J. A. Miwa, C. Cacho, R. T. Chapman, E. Springate, F. Fromm *et al.*, Tunable carrier multiplication and cooling in graphene, *Nano Lett.* **15**, 326 (2015).
- [29] M. Dendzik *et al.*, Observation of an Excitonic Mott Transition Through Ultrafast Core-cum-Conduction Photoemission Spectroscopy, *Phys. Rev. Lett.* **125**, 096401 (2020).
- [30] M. K. Man, J. Madéo, C. Sahoo, K. Xie, M. Campbell, V. Pareek, A. Karmakar, E. L. Wong, A. Al-Mahboob, N. S. Chan *et al.*, Experimental measurement of the intrinsic excitonic wave function, *Sci. Adv.* **7**, eabg0192 (2021).
- [31] S. Dong, M. Puppini, T. Pincelli, S. Beaulieu, D. Christiansen, H. Hübener, C. W. Nicholson, R. P. Xian, M. Dendzik, Y. Deng *et al.*, Direct measurement of key exciton properties: Energy, dynamics, and spatial distribution of the wave function, *Nat. Sci.* **1**, e10010 (2021).
- [32] Z. Nie, R. Long, L. Sun, C.-C. Huang, J. Zhang, Q. Xiong, D. W. Hewak, Z. Shen, O. V. Prezhdo, and Z.-H. Loh, Ultrafast carrier thermalization and cooling dynamics in few-layer  $\text{MoS}_2$ , *ACS Nano* **8**, 10931 (2014).
- [33] E. Perfetto, D. Sangalli, A. Marini, and G. Stefanucci, Nonequilibrium Bethe-Salpeter equation for transient photoabsorption spectroscopy, *Phys. Rev. B* **92**, 205304 (2015).
- [34] See the Supplemental Material at <http://link.aps.org/supplemental/10.1103/PhysRevLett.128.016801> for details on the index convention, derivation of the ODE scheme, derivation of the BE scheme, and numerical implementation.
- [35] A. Marini, Competition between the electronic and phonon-mediated scattering channels in the out-of-equilibrium carrier dynamics of semiconductors: An ab-initio approach, *J. Phys. Conf. Ser.* **427**, 012003 (2013).
- [36] A. Steinhoff, M. Florian, M. Ršner, M. Lorke, T. O. Wehling, C. Gies, and F. Jahnke, Nonequilibrium carrier dynamics in transition metal dichalcogenide semiconductors, *2D Mater.* **3**, 031006 (2016).
- [37] E. Perfetto and G. Stefanucci, CHEERS: A tool for correlated hole-electron evolution from real-time simulations, *J. Phys. Condens. Matter* **30**, 465901 (2018).
- [38] M. Kira and S. Koch, Many-body correlations and excitonic effects in semiconductor spectroscopy, *Prog. Quantum Electron.* **30**, 155 (2006).
- [39] J. González, F. Guinea, and M. A. H. Vozmediano, Unconventional Quasiparticle Lifetime in Graphite, *Phys. Rev. Lett.* **77**, 3589 (1996).
- [40] E. H. Hwang, B. Y.-K. Hu, and S. Das Sarma, Inelastic carrier lifetime in graphene, *Phys. Rev. B* **76**, 115434 (2007).
- [41] Y. Pavlyukh, G. Stefanucci, and R. van Leeuwen, Dynamically screened vertex correction to  $GW$ , *Phys. Rev. B* **102**, 045121 (2020).
- [42] F. Rana, Electron-hole generation and recombination rates for coulomb scattering in graphene, *Phys. Rev. B* **76**, 155431 (2007).
- [43] E. Malic, T. Winzer, E. Bobkin, and A. Knorr, Microscopic theory of absorption and ultrafast many-particle kinetics in graphene, *Phys. Rev. B* **84**, 205406 (2011).
- [44] A. Tomadin, D. Brida, G. Cerullo, A. C. Ferrari, and M. Polini, Nonequilibrium dynamics of photoexcited electrons in graphene: Collinear scattering, Auger processes, and the impact of screening, *Phys. Rev. B* **88**, 035430 (2013).

- [45] G. Alymov, V. Vyurkov, V. Ryzhii, A. Satou, and D. Svintsov, Auger recombination in dirac materials: A tangle of many-body effects, *Phys. Rev. B* **97**, 205411 (2018).
- [46] A. H. Castro Neto, F. Guinea, N. M. R. Peres, K. S. Novoselov, and A. K. Geim, The electronic properties of graphene, *Rev. Mod. Phys.* **81**, 109 (2009).
- [47] T. Ando, Screening effect and impurity scattering in monolayer graphene, *J. Phys. Soc. Jpn.* **75**, 074716 (2006).
- [48] A. Grüneis, R. Saito, G. G. Samsonidze, T. Kimura, M. A. Pimenta, A. Jorio, A. G. S. Filho, G. Dresselhaus, and M. S. Dresselhaus, Inhomogeneous optical absorption around the K point in graphite and carbon nanotubes, *Phys. Rev. B* **67**, 165402 (2003).
- [49] E. H. Hwang and S. Das Sarma, Dielectric function, screening, and plasmons in two-dimensional graphene, *Phys. Rev. B* **75**, 205418 (2007).
- [50] S. Schmitt-Rink, D. S. Chemla, and H. Haug, Nonequilibrium theory of the optical Stark effect and spectral hole burning in semiconductors, *Phys. Rev. B* **37**, 941 (1988).
- [51] J. R. Kuklinski and S. Mukamel, Optical properties of wannier excitons in the linear and weakly nonlinear regime, *Phys. Rev. B* **42**, 2959 (1990).
- [52] S. Glutsch and R. Zimmermann, Coherent optics for pumping near the absorption edge, *Phys. Rev. B* **45**, 5857 (1992).
- [53] P. Littlewood and X. Zhu, Possibilities for exciton condensation in semiconductor quantum-well structures, *Phys. Scr.* **1996**, 56 (1996).
- [54] T. Östreich and K. Schönhammer, Non-stationary excitonic-insulator states in photoexcited semiconductors, *Z. Phys. B Condens. Matter* **91**, 189 (1993).
- [55] K. Hannewald, S. Glutsch, and F. Bechstedt, Excitonic insulator through coherent pulse excitation? *J. Phys. Condens. Matter* **13**, 275 (2001).
- [56] S. Glutsch, F. Bechstedt, and R. Zimmermann, Optical excitation and bose condensation of excitons in low-dimensional systems, *Phys. Status Solidi (b)* **172**, 357 (1992).
- [57] E. Perfetto, D. Sangalli, A. Marini, and G. Stefanucci, Pump-driven normal-to-excitonic insulator transition: Josephson oscillations and signatures of BEC-BCS crossover in time-resolved ARPES, *Phys. Rev. Mater.* **3**, 124601 (2019).
- [58] R. E. Groenewald, M. Rösner, G. Schönhoff, S. Haas, and T. O. Wehling, Valley plasmonics in transition metal dichalcogenides, *Phys. Rev. B* **93**, 205145 (2016).
- [59] E. Perfetto, S. Bianchi, and G. Stefanucci, Time-resolved arpes spectra of nonequilibrium excitonic insulators: Revealing macroscopic coherence with ultrashort pulses, *Phys. Rev. B* **101**, 041201(R) (2020).
- [60] E. Perfetto and G. Stefanucci, Ultrafast creation and melting of nonequilibrium excitonic condensates in bulk WSe<sub>2</sub>, *Phys. Rev. B* **103**, L241404 (2021).
- [61] E. Perfetto, A. Marini, and G. Stefanucci, Self-consistent screening enhances the stability of the nonequilibrium excitonic insulator phase, *Phys. Rev. B* **102**, 085203 (2020).
- [62] G. Stefanucci and E. Perfetto, From carriers and virtual excitons to exciton populations: Insights into time-resolved ARPES spectra from an exactly solvable model, *Phys. Rev. B* **103**, 245103 (2021).
- [63] Y. Li, W. Liu, Y. Wang, Z. Xue, Y.-C. Leng, A. Hu, H. Yang, P.-H. Tan, Y. Liu, H. Misawa *et al.*, Ultrafast electron cooling and decay in monolayer WS<sub>2</sub> revealed by time-and energy-resolved photoemission electron microscopy, *Nano Lett.* **20**, 3747 (2020).
- [64] W. F. Brinkman and T. M. Rice, Electron-hole liquids in semiconductors, *Phys. Rev. B* **7**, 1508 (1973).
- [65] N. F. Mott, Metal-insulator transitions, *Contemp. Phys.* **14**, 401 (1973).
- [66] T. Rice, *The Electron-Hole Liquid in Semiconductors: Theoretical Aspects* (Academic Press, New York, 1978), pp. 1–86.
- [67] N. F. Mott, The basis of the electron theory of metals, with special reference to the transition metals, *Proc. Phys. Soc. London Sect. A* **62**, 416 (1949).
- [68] A. Steinhoff, M. Florian, M. Rösner, G. Schönhoff, T. O. Wehling, and F. Jahnke, Exciton fission in monolayer transition metal dichalcogenide semiconductors, *Nat. Commun.* **8**, 1166 (2017).